Lagrangian transport by deep-water surface gravity wavepackets: effects of directional spreading and stratification

C. Higgins[a,b], **T. S. van den Bremer**[a], **J. Vanneste**[b]

[a]Department of Engineering Science, University of Oxford, Oxford, OX1 3PJ, UK

[b]School of Mathematics and Maxwell Institute for Mathematical Sciences, University of Edinburgh, Edinburgh EH9 3FD, UK

(Received xx; revised xx; accepted xx)

The Lagrangian transport by surface gravity wavepackets consists of the Stokes drift and the wave-induced Eulerian return flow. We examine how directional spreading and density stratification affect this transport for a single wavepacket in deep water using a perturbation expansion. For an unstratified ocean, we show that the net displacement by the Eulerian return flow is finite, negative, the same at all vertical levels and inversely proportional to the depth for spanwise-infinite packets representing unidirectional (2D) seas, but zero for spanwise-localised packets representing directionally-spread seas (3D). We resolve this paradox by demonstrating that the transition between 2D-like (finite) and 3D-like (zero) displacement occurs on a time scale inversely proportional to the degree of directional spreading. For a stratified ocean, we show that in 2D the net displacement profile by the return flow oscillates slowly with depth, with a wavelength depending on the ratio of Brunt–Väisälä frequency to the surface wave group velocity and infinite displacements are predicted when the surface wavepacket resonantly excites internal waves. In 3D, the net displacement remains zero even in the presence of stratification, but the finite-time displacement may be appreciably altered. We estimate the magnitude of these effects for typical ocean conditions.

1. Introduction

The periodic motion of Lagrangian particles beneath surface gravity waves is subject to a small net drift in the direction of wave propagation, a phenomenon known as Stokes drift (Stokes 1847). In the ocean, this net motion provides a significant contribution to the trajectories of drifters (Röhrs *et al.* 2012), and must be accounted for in search and recovery missions such as for the 2014 MH370 airplane crash in the Indian Ocean (Trinanes *et al.* 2016). Stokes drift can be key in the local modelling of oil spills (Christensen & Terrile 2009; Drivdal *et al.* 2014; Jones *et al.* 2016) and plays a potentially important yet largely unexplored role in the near-surface transport and dispersion of plastic pollution (e.g. Lebreton *et al.* (2018)).

Since Stokes (1847), the classical drift for regular irrotational water waves has been extended to incorporate other physical effects. Longuet-Higgins (1953) introduced viscous boundary layers, showing that vorticity is eventually transported into the fluid interior and alters the mass transport profiles. In a rotating frame, Ursell & Deacon (1950) showed that the Lagrangian drift accompanying a periodic wave train must be zero, as an unopposed Stokes drift would violate conservation of circulation. Hasselmann (1970) demonstrated that rotation induces a cross-wave stress, causing Eulerian currents to rotate at the inertial frequency and to cancel the Stokes drift after half an inertial period.

Realistic sea states do not consist of regular waves but are made up from wavepackets (Longuet-Higgins 1957), a feature which is a consequence of linear superposition of waves of different wavenumbers and frequencies. Since Stokes drift depends on the square of the local wave amplitude, its associated mass transport becomes divergent on the packet-scale. Longuet-Higgins & Stewart (1962) demonstrated that a deep Eulerian return flow forms in response to this divergence. This Eulerian return flow also influences the nonlinear evolution of the wave envelope (Davey & Stewartson 1974; Dysthe 1979). The total Lagrangian velocity is given by the sum of the Stokes drift and the induced Eulerian flow ($\boldsymbol{u}_{\mathrm{L}} = \boldsymbol{u}_{\mathrm{E}} + \boldsymbol{u}_{\mathrm{S}}$, e.g. Bühler (2014)). For surface wavepackets in infinitely deep water, the sum of mass transports due to the Stokes and Eulerian flows is zero (e.g. McIntyre (1980)). Stokes drift is localised near the surface while the Eulerian return flow is more persistent with depth, so that packets induce a depth-dependent net transport of Lagrangian particles (e.g. van den Bremer & Taylor (2016)). Due to directional spreading of the underlying wave spectrum about a peak wavenumber, wavepackets frequently exhibit some localisation in the spanwise direction, and this may considerably reduce the magnitude of the return flow and its associated Eulerian displacement (e.g. van den Bremer & Taylor (2015)). Starting from the three-dimensional Eulerian mean flow computed by Hasselmann (1962), Herbers & Janssen (2016) computed the Lagrangian vertical and horizontal motions of a particle at the surface for an arbitrary wave spectrum. More recently, Haney & Young (2017) examined the propagation of a wavepacket on a stratified ocean, showing that density stratification significantly distorts the Eulerian return flow.

For a random wave field, the wave-induced Lagrangian transport results in a dispersion of particles that may be well-represented as a diffusion. This dispersion can be attributed to the interaction between random second-order Lagrangian flows (Herterich & Hasselmann 1982). Although the Eulerian wave-induced mean flow makes no contribution to particle dispersion in infinite depth (Herterich & Hasselmann 1982), recent work has emphasised its crucial importance for rotating shallow water (Bühler & Holmes-Cerfon 2009).

In this paper, we investigate the Lagrangian transport associated with a single deterministic spanwise-localised (or 3D) surface gravity wavepacket on a stratified ocean, focussing on the net transport by the Eulerian return flow. Throughout the paper we shall assume that directional spreading is relatively weak, so that the spanwise scale of the packet is greater than or equal to its characteristic scale in the direction of propagation; this is appropriate for swell conditions and for quasi-unidirectional sea states. We shall further assume that wavetrains are quasi-monochromatic or their spectra narrow-banded. Motivated by open-ocean applications, we also assume the surface waves have wavelengths much smaller than the water depth (i.e. are deep-water waves). We do not place such a restriction on the packet's characteristic length scale relative to the depth, and thus on the scale of the return flow. For an unstratified ocean, we use perturbation methods to demonstrate that the net displacement of particles by the Eulerian return flow is finite and depth-independent for a spanwise-infinite wavepacket (2D), but vanishes altogether for a spanwise-localised (3D) packet. In doing so, we correct erroneous numerical predictions by van den Bremer & Taylor (2016) of more complex 2D displacement profiles and by van den Bremer & Taylor (2015) of small yet non-zero displacements in 3D. We resolve the paradox of finite net displacements in 2D and zero net displacements in 3D by exploring displacements over finite time. While displacement underneath a 3D wavepacket is 2D-like (increasing) for small time, an opposing part of the Eulerian return flow returns a Lagrangian particle to its original position at later times. This opposing part of the Eulerian flow only forms in 3D when the flow may return around rather than beneath the packet. Reversal of the particle displacement occurs at a time that is proportional to the inverse of the spanwise packet-scale, occurring much later for almost-2D packets.

For a stratified ocean, we show that the net displacement profile by the return flow is (slowly) oscillatory function of depth in 2D, with a wavelength depending on the ratio of Brunt-Väisälä frequency N to the surface wave group velocity c_g. Large net displacements are predicted when the wavenumber N/c_g is close to an integer multiple of π/d (where d is the water depth), corresponding to an exact resonance between the surface wave group velocity and the phase velocity of an internal wave with zero horizontal wavenumber. In 3D, the net displacement remains zero even in the presence of stratification.

This paper is laid out as follows. First, §2 examines the unstratified case, distinguishing net displacement in 2D (§2.2), 3D (§2.3), and studying the transition between them over finite times (§2.4). Second, §3 addresses the stratified case, distinguishing net displacement in 2D (§3.2) and 3D (§3.3). We examine the implications of our results in §4 and draw conclusions. Appendix A explores the influence of the second-order set-down of the free surface on net displacement, and Appendix B considers the otherwise neglected impact of leading-order dispersion.

2. Unstratified flow

2.1. *Governing equations*

We begin by considering the unstratified case. A three-dimensional body of water of depth d and infinite lateral extent is assumed, with a coordinate system (x,y,z), where x and y denote the horizontal coordinates, and z the vertical coordinate measured from the undisturbed water level upwards. Inviscid, incompressible and irrotational flow in the absence of Coriolis forces and stratification is assumed; as a result, the velocity vector can be written as the gradient of the velocity potential $\boldsymbol{u} = \boldsymbol{\nabla}\phi$. In addition to the no-flow condition at the bottom ($\partial_z\phi = 0$ at $z = -d$), the governing equation in the fluid interior (Laplace) and the kinematic and dynamic boundary conditions are

$$\left(\partial_x^2 + \partial_y^2 + \partial_z^2\right)\phi = 0, \quad \partial_z\phi\,|_{z=h} = \partial_t h + \boldsymbol{\nabla}_{\mathrm{H}}\phi|_{z=h}\cdot\boldsymbol{\nabla}_{\mathrm{H}}h, \quad \partial_t\phi|_{z=h} + gh + \frac{1}{2}|\boldsymbol{\nabla}\phi|^2\,|_{z=h} = 0, \tag{2.1a,b,c}$$

where the free surface elevation is denoted by $z = h(x,y,t)$ and $\boldsymbol{\nabla}_{\mathrm{H}}$ is the horizontal gradient.

The wave amplitude is assumed small: $\alpha \equiv a_0k_0 \ll 1$, where a_0 is the peak amplitude of the free surface elevation and k_0 the wavenumber of the carrier wave. We solve the set (2.1) using a Stokes expansion and consider the first two orders, so that $\phi = \phi_1 + \phi_2 + ...$ and $h = h_1 + h_2 + ...$, with the subscript denoting the order in α.

2.1.1. *First-order solutions:* $O(\alpha)$

We assume that the ocean is deep with respect to the waves ($k_0d \gg 1$), and that the packet is quasi-monochromatic, weakly localised in the y-direction, and propagates along the x-axis, so that the first-order solution takes the form

$$h_1 = \mathrm{Re}\left[A_0(\varepsilon\tilde{x}, \varepsilon Ry, \varepsilon^2 t)e^{i\theta(x,t)}\right] + O(\alpha\varepsilon), \tag{2.2a}$$

$$\phi_1 = \mathrm{Re}\left[-\frac{i\omega_0}{k_0}A_0(\varepsilon\tilde{x}, \varepsilon Ry, \varepsilon^2 t)e^{i\theta(x,t)}e^{k_0 z}\right] + O(\alpha\varepsilon), \tag{2.2b}$$

where $\theta = k_0x - \omega_0 t$ with $\omega_0 = \sqrt{gk_0}$ denoting the angular frequency, and $\tilde{x} \equiv x - c_g t$ denotes the coordinate in a frame moving with the group velocity c_g. The amplitude scale is $a_0 \equiv ||A_0||$. Slow variation and weak spanwise localisation of the packet are captured by the bandwidth parameter $\varepsilon \equiv (2k_0\sigma_x)^{-1} \ll 1$ and the aspect ratio $R \equiv \sigma_x/\sigma_y$, where σ_x and σ_y are the characteristic packet scales in x (length) and in y (width), respectively. The limit $\varepsilon \to 0$ recovers the case of a periodic wave. Throughout this paper, we consider only weak localisation in y, so that the packet is wider than it is long, and hence R lies between 0 (a 2D packet) and 1 (a round packet). In §2.4 we explore the influence of R on the finite-time displacement by the return flow. The terms of $O(\alpha\varepsilon)$ in (2.2a,b) are not needed to compute the leading-order wave-induced forcing, but need to be considered when assessing the effect of dispersion that arises via the $\varepsilon^2 t$-dependence (see Appendix B).

The Stokes drift is a wave property and can be calculated directly from the linear solution (2.2) as

$$\boldsymbol{u}_{\mathrm{S}} = \overline{\boldsymbol{\Delta x}_1 \cdot \boldsymbol{\nabla u}_1} = k_0 \left(\omega_0 |A_0|^2, 0, -\frac{3}{2}\varepsilon c_g \partial_{\tilde{x}} |A_0|^2 \right) e^{2k_0 z} + O(\alpha^2\varepsilon^2), \tag{2.3}$$

where the overbar represents an average over the wave phase, and $\boldsymbol{\Delta x}_1 = \int \boldsymbol{u}_1 dt$.

2.1.2. *Second-order solutions: $O(\alpha^2)$*

The Eulerian return flow is not a wave property, but is found by solving the wave-averaged governing equations at second order in steepness. Expanding (2.1b,c) about the undisturbed level $z = 0$, retaining terms up to quadratic and wave-averaging yields forcing equations for the mean flow and the wave-averaged free surface (cf. Longuet-Higgins & Stewart (1962); McAllister *et al.* (2018)),

$$\left(\frac{1}{g}\partial_t^2 + \partial_z \right) \phi_2 = \boldsymbol{\nabla}_{\mathrm{H}} \cdot \overline{(\boldsymbol{u}_1 h_1)} - \overline{\frac{1}{g}\partial_t \left(h_1 \partial_{tz}\phi_1 + \frac{1}{2}|\boldsymbol{\nabla}\phi_1|^2 \right)} \Bigg|_{z=0}, \tag{2.4}$$

$$h_2 = -\frac{1}{g} \left(\partial_t \phi_2 + \overline{\left(h_1 \partial_{tz}\phi_1 + \frac{1}{2}|\boldsymbol{\nabla}\phi_1|^2 \right)} \right) \Bigg|_{z=0}, \tag{2.5}$$

where we omit overbars on second-order quantities as we focus on mean quantities only. The first term on the right-hand side of (2.4) is the forcing due to the divergence of the transport $\boldsymbol{M}$ associated with the waves, explicitly defined here as

$$\boldsymbol{M} \equiv \overline{(\boldsymbol{u}_1 h_1)} = \int_{-d}^{0} \boldsymbol{u}_{\mathrm{S}} dz, \tag{2.6}$$

which for surface waves can be expressed as the depth-integrated mass flux associated with the Stokes drift (the second equality; e.g., §4 of McIntyre (1981)). We refer to $\boldsymbol{M}$ in this paper as the Stokes transport. The second term on the right-hand side of (2.4) can be understood as the effect of the set-down of the wave-averaged free surface h_2 on the return flow. In deep water ($k_0 d \gg 1$), this set-down does not contribute to the forcing of the return flow to leading order, as is evident from substituting the linear polarisation relationships into the second term on the right-hand side of (2.4). Furthermore, the double time derivative on the left-hand side of (2.4) can be ignored when $k_0 d \gg 1$ and the return flow arises solely from the divergence of the Stokes transport (cf. a rigid-lid approximation, see also the discussion in appendix A). Equation (2.4) then simplifies to

$$\partial_z \phi_2 (\tilde{x}, y, 0) = \partial_{\tilde{x}} M + O\left(\alpha^2 \varepsilon^2\right), \tag{2.7}$$

where M is the x-component of $\boldsymbol{M}$.

2.2. *Unstratified flow in 2D*

For two-dimensional flows, we make use of the streamfunction ψ, implicitly defined by $\boldsymbol{u}_2 = \boldsymbol{\nabla} \times (\psi_2 \hat{\boldsymbol{y}})$ and satisfying a Laplace boundary-value problem. The surface value of the streamfunction is the Stokes transport, and the ocean floor is a streamline:

$$\left(\partial_{\tilde{x}}^2 + \partial_z^2\right)\psi_2 = 0, \qquad \psi_2\left(\tilde{x}, 0\right) = M, \qquad \psi_2\left(\tilde{x}, -d\right) = 0. \tag{2.8a,b,c}$$

We are interested in the net (or long-time) Eulerian displacement by the return flow,

$$\Delta x_{\mathrm{E}} = \int_{-\infty}^{\infty} u_2 dt = \frac{1}{c_g}\int_{-\infty}^{\infty} u_2 d\tilde{x}, \tag{2.9}$$

where the second equality makes use of the translating reference frame of the wavepacket. We can compute the net displacement in (2.9) without explicitly evaluating ψ_2. First, we integrate (2.8) over all $\tilde{x}$, noting that the vertical velocity $\partial_{\tilde{x}}\psi_2$ is zero at infinity, which reduces (2.8a) to the ordinary differential equation

$$\frac{d^2}{dz^2}\int_{-\infty}^{\infty}\psi_2 d\tilde{x} = 0, \quad \text{with} \quad \left.\int_{-\infty}^{\infty}\psi_2 d\tilde{x}\right|_{z=0} = \int_{-\infty}^{\infty} M d\tilde{x}, \qquad \left.\int_{-\infty}^{\infty}\psi_2 d\tilde{x}\right|_{z=-d} = 0, \tag{2.10a,b,c}$$

as boundary conditions. The solution is

$$\int_{-\infty}^{\infty}\psi_2\left(\tilde{x}, z\right) d\tilde{x} = \left(\frac{z+d}{d}\right)\int_{-\infty}^{\infty} M d\tilde{x}, \tag{2.11}$$

and the net displacement is deduced by dividing by c_g and taking the negative z-derivative (from (2.9), noting $u_2 = -\partial_z\psi_2$),

$$\Delta x_{\mathrm{E}} = -\frac{1}{c_g}\partial_z\int_{-\infty}^{\infty}\psi_2\left(\tilde{x}, z\right) d\tilde{x} = -\frac{1}{c_g d}\int_{-\infty}^{\infty} M d\tilde{x}. \tag{2.12}$$

We thus obtain the perhaps surprising result that the net displacement by the return flow is independent of depth. The displacement is finite and negative, unless the depth is truly infinite (not just $k_0 d \gg 1$), when it goes to zero. The result does not rely on any assumptions related to the depth dependence of the return flow (we have assumed the waves are deep, i.e. $k_0 d \gg 1$).

The net Lagrangian displacement $\Delta x_{\mathrm{L}} \equiv \Delta x_{\mathrm{E}} + \Delta x_{\mathrm{S}}$ is depth-dependent, and is obtained by integrating (2.3) with respect to time and adding to (2.12) to find

$$\Delta x_{\mathrm{L}} = \frac{\alpha^2\sqrt{\pi}}{k_0}\left(2k_0\sigma_x e^{2k_0 z} - \frac{\sigma_x}{d}\right), \tag{2.13}$$

where we have assumed a Gaussian packet $A_0 = a_0\exp\left(-\tilde{x}^2/(2\sigma_x^2)\right)$, resulting in the surface forcing $M = \omega_0 a_0^2\exp\left(-\tilde{x}^2/\sigma_x^2\right)/2$, and $\alpha = a_0 k_0$ denotes wave steepness. Lagrangian particles are displaced forwards above a certain depth and backwards beneath it. Depth-integrating (2.13) from $-d$ to 0 gives the total volume transported by the Lagrangian flow, which vanishes in the limit $k_0 d \gg 1$ considered here. Whenever we assume Gaussian packets, displacements will be scaled by the factor $\alpha^2\sqrt{\pi}/k_0$, as denoted by a star,

$$\Delta x_{\mathrm{E}}^* \equiv k_0\Delta x_{\mathrm{E}}/(\alpha^2\sqrt{\pi}), \qquad \Delta x_{\mathrm{S}}^* \equiv k_0\Delta x_{\mathrm{S}}/(\alpha^2\sqrt{\pi}), \qquad \Delta x_{\mathrm{L}}^* \equiv k_0\Delta x_{\mathrm{L}}/(\alpha^2\sqrt{\pi}), \tag{2.14a,b,c}$$

so that $\Delta x_{\mathrm{E}}^* = -1/d^*$ with $d^* = d/\sigma_x$.

2.3. *Unstratified flow in 3D*

Unlike in the two-dimensional case, we must explicitly solve for the return flow before we can evaluate the associated net displacement in 3D. We use a double Fourier transform in $\tilde{x}$ and y to obtain the potential

$$\phi_2(\tilde{x}, y, z) = \frac{1}{4\pi^2}\mathrm{Re}\iint_{\mathbb{R}^2} \frac{ik\hat{M}}{\sqrt{k^2+l^2}} \frac{\cosh((z+d)\sqrt{k^2+l^2})}{\sinh(d\sqrt{k^2+l^2})} e^{ik\tilde{x}} e^{ily} dk dl, \tag{2.15}$$

where $\hat{M}$ is the Fourier transform of M. To find the net Eulerian displacement, we take the x-derivative of (2.15) to obtain u_2 and integrate over all time (here $\tilde{x}$), resulting in a delta-function in k, which evaluates to zero:

$$\Delta x_{\mathrm{E}} = -\frac{1}{2\pi c_g}\mathrm{Re}\iint_{\mathbb{R}^2} \delta(k) \frac{k^2\hat{M}}{\sqrt{k^2+l^2}} \frac{\cosh((z+d)\sqrt{k^2+l^2})}{\sinh(d\sqrt{k^2+l^2})} e^{ily} dk dl = 0. \tag{2.16}$$

This result (the net Eulerian displacement is zero in 3D) is in stark contrast with the negative, depth-independent net displacement in 2D (2.12). We can also obtain this result from consideration of irrotationality of the return flow,

$$\partial_y w_2 = \partial_z v_2, \qquad \partial_z u_2 = \partial_x w_2, \qquad \partial_y u_2 = \partial_x v_2. \tag{2.17a,b,c}$$

Integrating (2.17b,c) over all time (equivalently, $\tilde{x}$), and assuming the velocity components v_2 and w_2 decay sufficiently rapidly far from the packet ($|\tilde{x}| \to \infty$), we obtain the conditions

$$\partial_z \Delta x_{\mathrm{E}} = 0, \qquad \partial_y \Delta x_{\mathrm{E}} = 0, \tag{2.18a,b}$$

which together imply the net displacement Δx_{E} is at most a constant. As we require the flow to decay far from the packet in y, we immediately obtain the result that $\Delta x_{\mathrm{E}} = 0$.

Physical insight into this paradox may be obtained from mass balance arguments. Depth-integrating the incompressibility condition ($\boldsymbol{\nabla} \cdot \boldsymbol{u}_2 = 0$), we obtain

$$\partial_{\tilde{x}} \int_{-d}^{0} (u_2 + u_{\mathrm{S}})\, dz = -\partial_y \int_{-d}^{0} v_2 dz, \tag{2.19}$$

where we have used the boundary conditions for w_2 at the bottom and at the free surface (2.7), and we have rewritten M as the vertical integral of the Stokes drift (cf. (2.6)). Thus the divergence of the Lagrangian mass flux in the propagation direction is counterbalanced by a mass flux in the transverse direction. The return flow in 3D is not local to the packet and extends into the unbounded y-direction, while Stokes drift is confined to the 'footprint' of the packet near the surface. Mass may return around rather than beneath the packet, with the result that Lagrangian particles experience no net displacement by the return flow. In fact, the area integral of the Lagrangian velocity is zero, which may be seen by y-integrating (2.19). Even though the net Eulerian displacement is zero at any point, the area integration of the Eulerian displacement must balance the area integration of the Stokes drift displacement. Mathematically, the time and area integrals do not commute. By contrast, there is no such paradox for the Stokes drift; since it is depth-limited and inherits the envelope decay of the packet, the associated net displacement decays rapidly in both y and z. We will now explore the finite-time displacement.

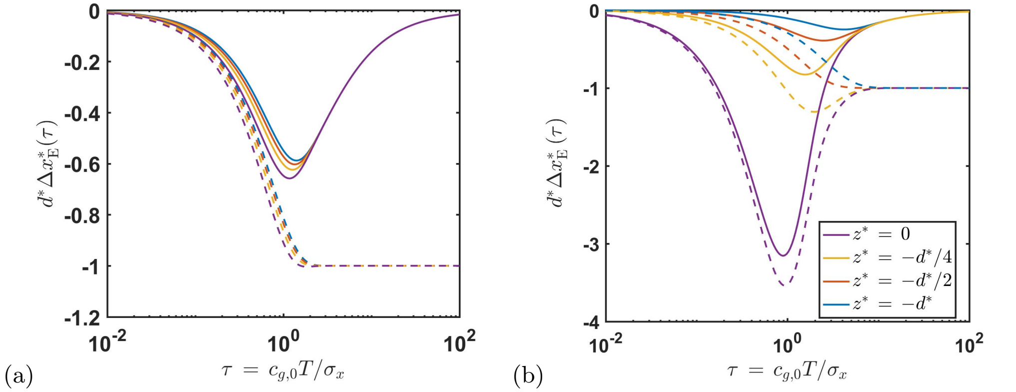

FIGURE 1. Scaled finite-time Eulerian displacement for an unstratified flow at different depths, obtained from numerical integration of (2.22): the solid lines correspond to a 3D flow with $R = \sigma_x/\sigma_y = 1/3$, and the dashed lines to a 2D flow ($R = 0$). Panel (a) shows the displacement for a shallower return flow ($d^* \equiv d/\sigma_x = 0.5$), and panel (b) for a deeper return flow ($d^* = 5$).

2.4. *Finite-time displacement and the 2D-3D transition*

We define the finite-time displacement as the symmetric time integral

$$\Delta x_{\mathrm{E}}(T) = \int_{-T}^{T} u_2 dt = \frac{1}{c_g}\int_{-c_{g,0}T}^{c_{g,0}T} u_2 d\tilde{x}, \tag{2.20}$$

where $T = 0$ corresponds to $\tilde{x} = 0$, and we choose $y = 0$, thereby examining a particle underneath the centre of the packet. Notationally, we distinguish the finite-time displacement $\Delta x_{\mathrm{E}}(T)$ in (2.20) from its long-time limit Δx_{E} in (2.9) by including its explicit dependence on time. We will choose the surface forcing M, and thereby its Fourier transform $\hat{M}$, to be Gaussian,

$$M = \frac{\omega_0 a_0^2}{2} e^{-\tilde{x}^2/\sigma_x^2} e^{-y^2/\sigma_y^2}, \qquad \hat{M} = \frac{\omega_0 a_0^2 \sigma_x \sigma_y \pi}{2} e^{-k^2\sigma_x^2/4} e^{-l^2\sigma_y^2/4}. \tag{2.21a,b}$$

Differentiating (2.15) with respect to $\tilde{x}$ to obtain u_2 and integrating as in (2.20), we obtain after changing from dimensional variables to the nondimensional variables $\mu \equiv k c_g T$ and $\lambda \equiv l\sigma_y$,

$$\Delta x^*_{\mathrm{E}}(\tau) = \frac{-1}{2\pi^{3/2}\tau} \mathrm{Re} \iint_{\mathbb{R}^2} \frac{\mu \sin(\mu)}{\sqrt{\mu^2 + (R\tau)^2\lambda^2}} e^{-\mu^2/(4\tau^2)} e^{-\lambda^2/4} \times \frac{\cosh\left((z^* + d^*)\sqrt{\mu^2 + (R\tau)^2\lambda^2}/\tau\right)}{\sinh\left(d^*\sqrt{\mu^2 + (R\tau)^2\lambda^2}/\tau\right)} d\mu d\lambda, \tag{2.22}$$

where we have introduced the dimensionless packet time scale $\tau \equiv c_g T/\sigma_x$, $d^* \equiv d/\sigma_x$, and the packet aspect ratio $R \equiv \sigma_x/\sigma_y$ ($R \to 0$ corresponds to 2D). Unlike its long-time limit, the finite-time displacement depends on $z^* \equiv z/\sigma_x$.

Figure 1 illustrates the finite-time Eulerian displacements obtained by numerical integration of (2.22) for particles at various depths in a 3D flow ($R = 1/3$), comparing these to their 2D counterparts ($R = 0$). We plot $d^*\Delta x^*_{\mathrm{E}}(\tau)$ on the y-axis, so that the 2D long-time limit corresponds to -1 (cf. (2.13), (2.14a)). It is evident from this figure that the behaviour for small time is 2D-like, with the continuous lines (3D) tending towards zero and the dashed lines (2D) to -1 for large time, as previously discussed.

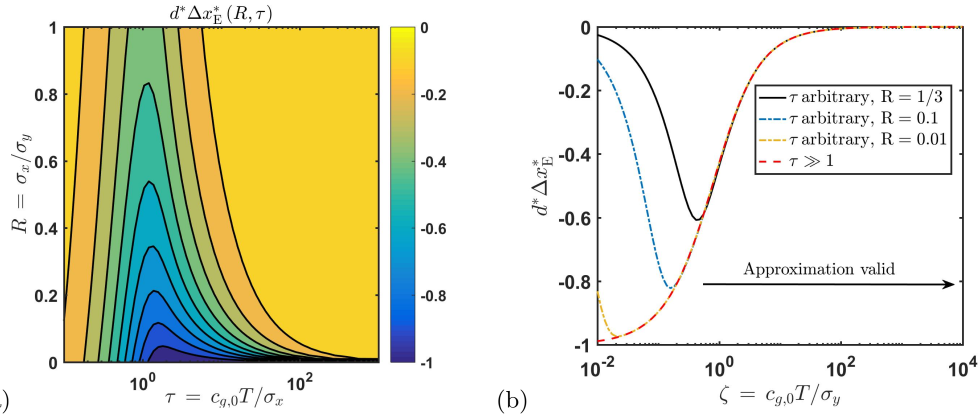

FIGURE 2. Finite-time Eulerian displacement for unstratified flow: contour plot as a function of aspect ratio R and packet time τ from numerical integration of (2.20) (panel (a)), and displacement obtained by numerical integration of (2.23) for three aspect ratios $R = \sigma_x/\sigma_y = 1/3, 0.1, 0.01$ (continuous black and dash-dotted blue and yellow lines, respectively) and (2.27) (red dashed line) as a function of $\zeta = R\tau = c_{g,0}T/\sigma_y$ (panel (b)).

The two panels compare a shallower return flow ($d^* = 0.5$) and a deeper return flow ($d^* = 5$). Whereas the 2D finite-time displacement is monotonic for shallower return flows, it can overshoot near the surface for deeper returns flows, reflecting the strong negative displacement underneath the centre of the packet being partly balanced by positive displacement near the surface at the packet's leading and trailing edges, which is absent in shallower return flows.

As insightful closed-form solutions to (2.22) do not exist, we consider the limiting case of a shallow return flow, corresponding to $d^* = d/\sigma_x \ll 1$. In this limit, the return flow's vertical variation is negligible, and (2.22) takes the form

$$\Delta x^*_{\mathrm{E}}(\tau) = -\frac{2}{d^*\pi^{3/2}}\int_0^\infty\int_0^\infty \frac{\mu\sin(\mu)}{\mu^2+(R\tau)^2\lambda^2}e^{-\mu^2/(4\tau^2)}e^{-\lambda^2/4}d\mu d\lambda. \tag{2.23}$$

The integral over λ may be performed analytically, yielding a single integral over μ,

$$\Delta x^*_{\mathrm{E}}(\tau,R) = -\frac{2}{d^*\sqrt{\pi}}\int_0^\infty \frac{\sin\mu}{\mu}e^{-\mu^2/(4\tau^2)}f(\mu/(2R\tau))\,d\mu, \tag{2.24}$$

where the function $f(t) \equiv t\exp(t^2)\,\mathrm{erfc}(t)$ for an arbitrary argument t. The function $f(\mu/(2R\tau))$ in (2.24) captures how the finite-time displacement varies with the aspect ratio R. Relevant small and large $R\tau$ limits of this function are

$$\lim_{R\tau\to 0} f\left(\frac{\mu}{2R\tau}\right) = \frac{1}{\sqrt{\pi}}, \qquad \lim_{R\tau\to\infty} f\left(\frac{\mu}{2R\tau}\right) = 0. \tag{2.25a,b}$$

We can rewrite (2.24) in a more instructive form, as the sum of two integrals

$$\begin{aligned}\Delta x^*_{\mathrm{E}}(\tau,R) = &-\frac{2}{d^*\sqrt{\pi}}\int_0^\infty e^{-\mu^2/(4\tau^2)}\frac{\sin\mu}{\mu}\left(f\left(\frac{\mu}{2R\tau}\right)-\frac{1}{\sqrt{\pi}}\right)d\mu\\ &-\frac{2}{d^*\pi}\int_0^\infty e^{-\mu^2/(4\tau^2)}\frac{\sin\mu}{\mu}d\mu,\end{aligned} \tag{2.26}$$

where the second integral now corresponds to the 2D finite-time displacement. To examine the long-time behaviour, we assume that $\tau \gg 1$, so that the second integral in (2.26) approaches the 2D net displacement $-1/d^*$, and the exponential function in the first integral can be set to 1. The displacement is then a function of a single parameter, $\zeta \equiv R\tau = c_g T/\sigma_y$, which corresponds to time scaled on the packet's width σ_y rather than its length σ_x, and we obtain

$$\Delta x^*_{\mathrm{E}}(\zeta) = -\frac{2}{d^*\sqrt{\pi}} \int_0^\infty \frac{\sin\mu}{\mu}\left(f\left(\frac{\mu}{2\zeta}\right) - \frac{1}{\sqrt{\pi}}\right) d\mu - \frac{1}{d^*}. \tag{2.27}$$

Therefore, 2D-like behaviour occurs for $\zeta \ll 1$ ($\tau \ll 1/R$), while 3D-like behaviour occurs for $\zeta \gg 1$ ($\tau \gg 1/R$) (cf. (2.25)). Physically, displacement remains 2D-like for a longer period of time when the packet's aspect ratio R is small and the packet is almost 2D. Figure 2(a) shows contours plots of the finite-time Eulerian displacement by a shallow return flow obtained from numerically integrating (2.20), demonstrating that the maximum negative displacement by the return flow occurs on a packet time scale of $\tau = O(1)$. Figure 2(b), compares numerical integration of (2.23) and its large τ-limit (2.27). Whereas the maximum negative displacement occurs at $\tau = O(1)$, the transition between 2D and 3D-like behaviour occurs when $\zeta = O(1)$, and 2D-like behaviour can thus last for a long time for small degrees of localisation in y (small R or near unidirectional packets).

We note in passing that the incorrect non-zero values of net displacement by the Eulerian return flow obtained from numerical integration in van den Bremer & Taylor (2016) (2D, infinite depth) and van den Bremer & Taylor (2015) (3D) resulted from insufficiently large limits on the integrals; these limits may need to be as large as $O(10^2)$-$O(10^3)$ packet time scales for small R, as illustrated in figure 2.

3. Stratified flow

3.1. *Governing equations*

In this section, we consider propagation of inviscid and incompressible surface waves on a stratified fluid. To include density stratification effects, we decompose the varying density as (Phillips 1977)

$$\rho = \rho_0 \left(1 + \frac{1}{g}\int_z^0 N^2(z')dz' - \frac{b}{g}\right), \tag{3.1}$$

where $b(x, y, z, t) = -g\Delta\rho/\rho_0$ is the buoyancy perturbation, and N is the Brunt-Väisälä frequency, which we assume to be constant. Invoking the Boussinesq approximation by neglecting density differences unless they result in a body force, the governing equations in the presence of stratification are (e.g. Haney & Young 2017)

$$\boldsymbol{\nabla}\cdot\boldsymbol{u} = 0, \qquad \partial_t\boldsymbol{u} + \boldsymbol{u}\cdot\boldsymbol{\nabla}\boldsymbol{u} = -\boldsymbol{\nabla}p + b\hat{\boldsymbol{z}}, \qquad \partial_t b + \boldsymbol{u}\cdot\boldsymbol{\nabla}b + wN^2 = 0, \tag{3.2a,b,c}$$

where p is the departure from hydrostatic pressure. The system (3.2) must be solved subject to dynamic and kinematic boundary conditions at the surface. Only the dynamic boundary condition ($p_{\mathrm{tot}} = 0$ at $z = h(x, y, t)$, where p_{tot} is the total pressure) is modified by density stratification, and we have, correct to second order, Haney & Young (2017)

$$w = \partial_t h + \boldsymbol{u}_{\mathrm{H}}\cdot\boldsymbol{\nabla}_{\mathrm{H}}h\Big|_{z=0}, \qquad p + h\partial_z p = gh + N^2h^2/2\Big|_{z=0}. \tag{3.3a,b}$$

We solve the set (3.2)-(3.3) using a Stokes expansion as for unstratified flow.

3.1.1. *First-order solutions: $O(\alpha)$*

Following Haney & Young (2017), we neglect the buoyancy force and the vorticity it generates in the first-order equations. From the linearised equation (3.2c) and boundary condition (3.3a), we have $b_1 \sim -N^2 h_1$. Taking the curl of the linearised (3.2b), we thus obtain for the non-dimensional vorticity

$$\frac{|\boldsymbol{\nabla} \times \boldsymbol{u}_1|}{k_0 a_0 \omega_0} \sim \frac{|\left(\hat{\boldsymbol{z}} \times \boldsymbol{\nabla}_{\mathrm{H}}\right) b_1|}{k_0 a_0 \omega_0^2} \sim \frac{N^2}{\omega_0^2}, \tag{3.4}$$

from which it is evident that vorticity is small when $(N/\omega_0)^2$ is small, and linear solutions may be treated as irrotational. For surface gravity waves in the ocean, $(N/\omega_0)^2$ is at most $O(10^{-3})$ (see table 1 for typical parameter values).

3.1.2. *Second-order solutions: $O(\alpha^2)$*

At second order, the mean flow is not irrotational, as the wave-averaged buoyancy b_2 is retained. Wave-averaging and defining wave-adjusted pressure to be $\varpi_2 \equiv p_2 + \overline{|\mathbf{u}_1|^2}/2$, the mean flow equations are Haney & Young (2017)

$$\boldsymbol{\nabla} \cdot \boldsymbol{u}_2 = 0, \qquad \partial_t \boldsymbol{u}_2 = -\boldsymbol{\nabla} \varpi_2 + b_2 \hat{\boldsymbol{z}}, \qquad \partial_t b_2 = -w_2 N^2. \tag{3.5a,b,c}$$

Assuming propagation along the x-axis, and using the (irrotational) linear solutions to rewrite $h_1 \partial_z p_1 = |\boldsymbol{u}_1|^2/2$ at $z = 0$, we may rewrite the surface boundary conditions (3.3) using the wave-adjusted pressure as

$$w_2|_{z=0} = \partial_t h_2 + \partial_x M, \qquad \varpi_2|_{z=0} = g h_2 + N^2 \overline{{h_1}^2}/2, \tag{3.6a,b}$$

where M is the x-component of $\boldsymbol{M}$ defined in (2.6). After eliminating all variables in favour of the vertical velocity w_2, and making the rigid-lid assumption in (3.6a) (valid for $k_0 d \gg 1$), the original problem (3.5) is reduced to solving an evolution equation for w_2 subject to the surface forcing and no-flow bottom boundary condition,

$$\left(\partial_t^2 \Delta + N^2 \Delta_{\mathrm{H}}\right) w_2 = 0, \qquad w_2|_{z=0} = \partial_{\tilde{x}} M, \qquad w|_{z=-d} = 0. \tag{3.7a,b,c}$$

Whereas Haney & Young (2017) used a modal expansion to explore the structure of the mean flow described by (3.7), we will instead solve using Fourier transforms, as this allows us to find displacements more easily. If N is sufficiently large, (3.6) allows for internal wave solutions. To ensure such internal waves lie in the packet's wake, we invoke causality, assuming the packet amplitude has been growing from $t = -\infty$ as $A_0(\tilde{x}, y) e^{\mu t}$ and then taking μ to zero from above.

3.2. *Stratified flow in 2D*

For two-dimensional flow, (3.7) can be solved in terms of a streamfunction ψ_2, where $w_2 = \partial_x \psi_2$. Moving into the reference frame of the packet, but accounting for causality so that $\partial_t = -c_g \partial_{\tilde{x}} + \mu$, we obtain from (3.7)

$$\left((\partial_{\tilde{x}} - \eta)^2 \left(\partial_{\tilde{x}}^2 + \partial_z^2\right) + q^2 \partial_{\tilde{x}}^2\right) \psi_2 = 0, \qquad \psi_2\left(\tilde{x}, 0\right) = M, \qquad \psi_2\left(\tilde{x}, -d\right) = 0, \tag{3.8a,b,c}$$

where $q \equiv N/c_g$ is the buoyancy wavenumber and $\eta \equiv \mu/c_g$. Equation (3.8a) is an evolution equation for the streamfunction depending on the stratification strength. To investigate the role of radiated internal waves, we use the Fourier transform instead of direct integration in $\tilde{x}$ as we did in the unstratified case (cf. (2.10)), and obtain after some manipulation

$$\psi_2 = \frac{1}{2\pi} \lim_{\eta \to 0^+} \int_{-\infty}^{\infty} \hat{M} \frac{\sinh\left((z+d)\sqrt{(k+i\eta)^2 - q^2}\right)}{\sinh\left(d\sqrt{(k+i\eta)^2 - q^2}\right)} e^{ik\tilde{x}} dk. \tag{3.9}$$

Interpreting (3.9) as an integral in the complex k-plane, the limit $\eta \to 0^+$ dictates that the integration contour lies slightly above the real axis. Note that (3.9) does not involve branch points, despite the presence of square roots, as the series expansion of the sinh / sinh function involves only even powers of $\sqrt{(k+i\eta)^2 - q^2}$. Taking the limit $\eta \to 0^+$, (3.9) reduces to a sum of convolution integrals between the (real-space) surface forcing M and the inverse transform of the sinh / sinh function, the latter being evaluated by summing over its poles on the real and imaginary axes,

$$\psi_2 = -\sum_{n=1}^{\lfloor qd/\pi \rfloor} \sin\left(\frac{n\pi z}{d}\right) \frac{n\pi}{k_n d^2} \int_{-\infty}^{\infty} M\left(x'\right) \sin\left(k_n\left(\tilde{x} - x'\right)\right) H\left(x' - \tilde{x}\right) dx' \\ - \sum_{n=\lceil qd/\pi \rceil}^{\infty} \sin\left(\frac{n\pi z}{d}\right) \frac{n\pi}{2\beta_2 d^2} \int_{-\infty}^{\infty} M\left(x'\right) e^{-\beta_n |\tilde{x} - x'|} dx', \quad (3.10)$$

where $\lfloor qd/\pi \rfloor$ and $\lceil qd/\pi \rceil$ respectively denote the floor and ceiling of qd/π, namely the closest integers below and above qd/π respectively; H is the Heaviside step function; $k_n = \sqrt{q^2 - n^2\pi^2/d^2}$ and $\beta_n^2 = -k_n^2$, and the real and imaginary poles of the sinh / sinh function in (3.9) are located at $\pm k_n$ and $\pm i\beta_n$, respectively (see also Haney & Young's (2017) modal solution).

When the stratification is sufficiently strong that $q > \pi/d$, poles located at $\pm k_n$ on the real k-axis correspond to an internal wave in the packet's wake. If instead $q < \pi/d$, the only poles present are those on the imaginary k-axis at $\pm i\beta_n$, giving rise to a purely evanescent mean flow.

In the far-field $|\tilde{x}| \to \infty$, we note that there are two different behaviours depending on the sign of $\tilde{x}$. Ahead of the packet where $\tilde{x} > 0$, and when $\tilde{x} \to \infty$, it may be seen from (3.10) that both of the convolution integrals above go to zero, so the oscillatory and evanescent portions of the flow disappear. Behind the packet ($\tilde{x} < 0$), the second integral in (3.10) vanishes in the far-field $\tilde{x} \to -\infty$, but the first may be completed to yield a purely oscillatory wake of internal waves,

$$\psi_2 \sim -\sum_{n=1}^{\lfloor qd/\pi \rfloor} \frac{n\pi}{k_n d^2} \sin\left(\frac{n\pi z}{d}\right) \operatorname{Im}\left(\hat{M}\left(k_n\right) e^{ik_n\tilde{x}}\right) \quad \text{as} \quad \tilde{x} \to -\infty, \quad (3.11)$$

where Im denotes the imaginary part of the expression within the square brackets (see equation (5.9) in Haney & Young (2017)).

To find the horizontal velocity, we take the negative z-derivative of (3.9) and find

$$u_2 = -\frac{1}{2\pi} \lim_{\eta \to 0^+} \int_{-\infty}^{\infty} \hat{M} \sqrt{(k+i\eta)^2 - q^2} \frac{\cosh\left((z+d)\sqrt{(k+i\eta)^2 - q^2}\right)}{\sinh\left(d\sqrt{(k+i\eta)^2 - q^2}\right)} e^{ik\tilde{x}} dk. \quad (3.12)$$

Integrating over time results in a delta-function centred at $k = 0$, as in the unstratified case. For a Gaussian packet, the net displacement is then given by

$$\Delta x^*_{\mathrm{E}} = -\frac{1}{d^*}(qd) \frac{\cos\left(qd(1 + z/d)\right)}{\sin\left(qd\right)}. \quad (3.13)$$

Unlike in the stratified case, the net displacement is now a function of both depth z and the parameter $qd = Nd/c_g$, which measures the ratio of the depth d to the vertical scale (c_g/N) of the $k_n = 0$ internal wave which would be forced were the ocean deep enough. Depth-profiles of the net displacement (3.13) are shown in figure 3 for different values of qd. We now explore the role of the stratification measure qd.

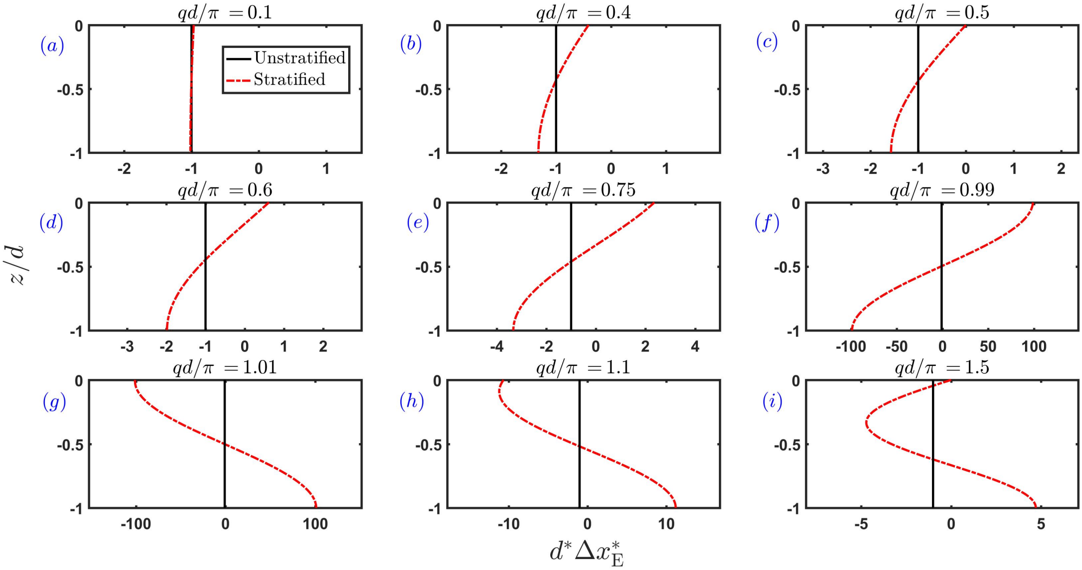

FIGURE 3. Rescaled net displacement $d^*\Delta x^*_{\mathrm{E}}$ by the return flow of a 2D packet in stratified flow from (3.13) as a function of depth z/d for various values of the stratification measure $qd = Nd/c_{g,0}$.

As $qd \to 0$, a Taylor expansion of (3.13) gives the dependence of net displacement on weak stratification

$$\Delta x^*_{\mathrm{E}} = -\frac{1}{d^*}\left(1 + \frac{q^2d^2}{6} - \frac{q^2d^2}{2}(1+z/d)^2 + O(qd)^3\right), \tag{3.14}$$

which recovers the unstratified case ($\Delta x^*_{\mathrm{E}} = -1/d^*$) if $qd \to 0$. To leading order, the net displacement is predicted to decrease in magnitude above a depth of $z/d = -(1-1/\sqrt{3}) \approx -0.42$, and increase in magnitude below, as is evident in figure 3(a)-(b).

If $qd = \pi/2$, the net Eulerian displacement remains negative and monotonic throughout the entire depth, but is zero at the surface,

$$d^*\Delta x^*_{\mathrm{E}} = -\frac{\pi}{2}\sin\left(\frac{\pi}{2}\frac{|z|}{d}\right). \tag{3.15}$$

This corresponds to the case in which stratification is sufficiently strong to quench the near-surface net Eulerian displacement, which is illustrated in figure 3(c). For $qd > \pi/2$, the net Eulerian displacement becomes positive near the surface (cf. figure 3(d)-(e)).

Only when $qd > \pi$ are internal waves generated in the packet's wake in 2D (figure 3(g)-(i)). This corresponds to $N > \pi c_g/d$. As qd traverses π (more generally $n\pi$), the displacement profile undergoes a change in sign (cf. figure 3(f)-(g)). When $qd \to n\pi$, with n a positive integer, the Eulerian displacement becomes singular (and very large in close proximity, cf. figure 3(f)-(g)). At the singular point, $c_g = Nd/n\pi$, representing a resonance in which the group velocity of the surface wavepacket matches the phase velocity of an internal wave with $k_n = \sqrt{q^2 - n^2\pi^2/d^2} = 0$. Note that $k_1 = 0$ is the border case between evanescent mean flow ($qd < \pi$) and internal-wave generation ($qd > \pi$) and, as a result, the horizontal velocity does not decay in $\tilde{x}$.

In real oceans, however, stratification tends to be too weak to satisfy $qd > \pi$, so 2D wavepackets are unlikely to excite internal waves (cf. table 1 and the discussion in

§4). Even if the stratification measure qd were close to π, e.g. for the largest depth and strongest stratification, the large displacements predicted by (3.13) are likely to be mitigated by dissipation, and we expect that large transfer of energy from the surface wavepacket to the internal wave wake would lead to disintegration of the packet.

The Stokes drift is unaltered by stratification when the waves are treated as irrotational, so the net Lagrangian displacement is obtained as the expression

$$\Delta x_{\mathrm{L}}^{*} = \left(2k_0\sigma_x e^{2k_0 z} - \frac{1}{d^*}\left(qd\right)\frac{\cos\left(qd\left(1+z/d\right)\right)}{\sin\left(qd\right)} \right). \tag{3.16}$$

Importantly, the depth integral of (3.16) from $-d$ to 0 remains zero, so the Eulerian flow still balances the transport of mass by the Stokes drift. Density stratification alters the manner in which the return flow transports mass without changing the vertically-integrated mass balance.

3.3. *Stratified flow in 3D*

The 3D problem is complicated by the addition of spanwise localisation of the packet, and because the return flow is not irrotational. The governing equation and associated boundary conditions for the vertical velocity are

$$\left(\partial_t^2\left(\partial_x^2+\partial_y^2+\partial_z^2\right)+N^2\left(\partial_x^2+\partial_y^2\right)\right)w_2 = 0, \qquad w_2|_{z=0} = \partial_x M, \qquad w_2|_{z=-d} = 0. \tag{3.17a,b,c}$$

Moving into the packet frame $\tilde{x}$ as before, and assuming constant Brunt–Väisälä frequency, the vertical velocity w_2 is obtained from (3.17) as the Fourier transform

$$w_2 = \frac{1}{4\pi^2}\lim_{\eta\to 0^+}\iint_{\mathbb{R}^2} ik\hat{M}\frac{\sinh\left((z+d)|\boldsymbol{k}|\beta_{\eta,q}(k)\right)}{\sinh\left(d|\boldsymbol{k}|\beta_{\eta,q}(k)\right)}e^{ik\tilde{x}}e^{ily}dkdl, \tag{3.18}$$

where we have adopted the compact notation

$$|\boldsymbol{k}| \equiv \sqrt{k^2+l^2}, \qquad \beta_{\eta,q}(k) \equiv \sqrt{\frac{(k+i\eta)^2-q^2}{(k+i\eta)^2}}. \tag{3.19a,b}$$

To obtain the horizontal velocity component u_2 from w_2 we first consider the curl of the momentum equation (3.5b), which connects vorticity generation to the rotated gradient of buoyancy,

$$\partial_t\left(\boldsymbol{\nabla}\times\boldsymbol{u}_2\right) = -\left(\hat{\boldsymbol{z}}\times\boldsymbol{\nabla}_{\mathrm{H}}\right)b_2 = \left(\partial_y b_2, -\partial_x b_2, 0\right), \tag{3.20}$$

from which it immediately follows that the vertical component of the vorticity is time-independent. Assuming this vanishes, $\partial_y u_2 - \partial_{\tilde{x}} v_2 = 0$; combining this with the incompressibility condition (3.5a) leads to a Poisson-like equation relating u_2 to w_2,

$$-\left(\partial_{\tilde{x}}^2+\partial_y^2\right)u_2 = \partial_{\tilde{x}}\partial_z w_2. \tag{3.21}$$

This is vacuously true in the unstratified case as it reduces to the Laplace equation (using $u_2 = \partial_x\phi_2$ and $w_2 = \partial_z\phi_2$), but nontrivial for a stratified flow. The transform $\hat{u}$ of u_2 may be found from $\hat{w}$ using (3.21) as $\hat{u} = ik\partial_z\hat{w}/(k^2+l^2)$. In real space, the horizontal velocity is hence given by the double Fourier transform

$$u_2 = -\frac{1}{4\pi^2}\lim_{\eta\to 0^+}\iint_{\mathbb{R}^2}\frac{k^2\hat{M}}{|\boldsymbol{k}|}\beta_{\eta,q}(k)\frac{\cosh\left((z+d)\,|\boldsymbol{k}|\beta_{\eta,q}(k)\right)}{\sinh\left(d|\boldsymbol{k}|\beta_{\eta,q}(k)\right)}e^{ik\tilde{x}}e^{ily}dkdl. \tag{3.22}$$

Recalling that $|\boldsymbol{k}|\sigma_x = \sqrt{\kappa^2+R^2\lambda^2}$, where $(\kappa,\lambda) \equiv (k\sigma_x, l\sigma_y)$ are dimensionless wavenumbers, setting $R \equiv \sigma_x/\sigma_y \to 0$ and subsequently taking $\eta \to 0^+$ recovers the 2D stratified case (3.10). Similarly, setting q to zero recovers the 3D unstratified case. As

$\eta \to 0^+$, equation (3.22) is dominated by the region in wavenumber space where the denominator vanishes, corresponding to 'resonant curves' defined by the condition

$$\lim_{\eta \to 0^+} d\sqrt{k^2 + (l_n(k))^2}\sqrt{\frac{q^2 - (k+i\eta)^2}{(k+i\eta)^2}} - n\pi = 0, \tag{3.23}$$

where $(k, l_n(k))$ are the coordinates of the resonant curve in the (k, l) plane for a particular integer $n > 0$, describing a resonance between the surface-wave group velocity and the phase speed of internal waves in the packet's wake (see Haney & Young 2017, (3.14)). Identifying these curves does not lead to meaningful analytical simplifications of the double Fourier transform defining u_2 in (3.22). Instead, we evaluate (3.22) numerically, with the causal η chosen to be small but nonzero.

Due to the stratification-dependent square root $\beta_{\eta,q}(k)$ defined in (3.19b), simple delta-function arguments, such as (2.16), for finding the net displacement from (3.22) become problematic: it is unclear from and (3.18) that $\hat{u}$ is well-defined at $k = 0$. Instead, time-integrating the z-component of vorticity in (3.21) gives $\partial_y \Delta x_{\mathrm{E}} = 0$, showing that in a 3D stratified ocean the net displacement by the return flow is y-independent, and hence is at most a function of z. Considering the limit $|y| \to \infty$ forces the net displacement to be globally zero, which is borne out in figure 4, where we show displacements evaluated by numerically time-integrating expression (3.22) for u_2 up to finite times. As incompressibility still holds, (2.19) indicates that mass-balance arguments are not fundamentally altered by the presence of an internal wave wake in 3D. Figure 4 shows that stratification effects enhance or diminish finite-time displacement in a similar way to 2D (cf. figure 3). Results in figure 4 are shown for realistic values of N, c_g and d, which are chosen to give the relatively large value of $qd/\pi = 0.6$ (see table 1). For this value of qd, the change in magnitude of finite-time Eulerian displacement can be appreciable, and this effect is most evident at depth. In this figure, the stratified 2D displacement in the long-time limit is positive at $z = 0$ and decreases monotonically with depth (cf. (3.15) and figure 3(d)). We note the persistence of 2D-like behaviour for small aspect ratios R (more evident at $z = -d/2$ and $z = -d$).

Finally, figure 5 summarises the combined effect of spanwise localisation and stratification by showing contours of the rescaled finite-time displacement as a function of the stratification measure qd/π and the packet aspect ratio R at different (packet) times $\tau = c_{g,0}t/\sigma_x$. To focus on what is realistic for the ocean, we vary the stratification measure qd/π between 0 and 0.6 (see table 1), so that stratification generally reduces the displacement near the surface and enhances it to become more negative at depth in the 2D-limit (cf. figure 3). At the surface (figure 5(a)-(c)), stratification does not have an effect at small time ($\tau = 1$), when displacements reach their peak values. At intermediate time ($\tau = 10$), the negative displacement is mainly reduced by the influence of spanwise localisation, and weakly by stratification. At large time ($\tau = 100$), displacements have practically vanished except for at very small aspect ratios R, recovering the 2D long-time limit as $R \to 0$. For these small values of R, stratification reduces displacements towards zero at the surface for $qd \leqslant \pi/2$, while this displacement becomes positive for $qd > \pi/2$, in accordance with the long-time limit (cf. figure 3(d)). At depth (figure 5(d)-(f)), we can observe the effect of stratification even for small time ($\tau = 1$) despite very small displacements at this time. At intermediate time ($\tau = 10$), the contours resembles those at small time ($\tau = 1$) albeit with larger magnitudes, as particles at the bottom begin to feel the flow but have not yet been affected by R. At large time ($\tau = 100$), displacements have again practically vanished other than for small aspect ratios R, recovering the 2D

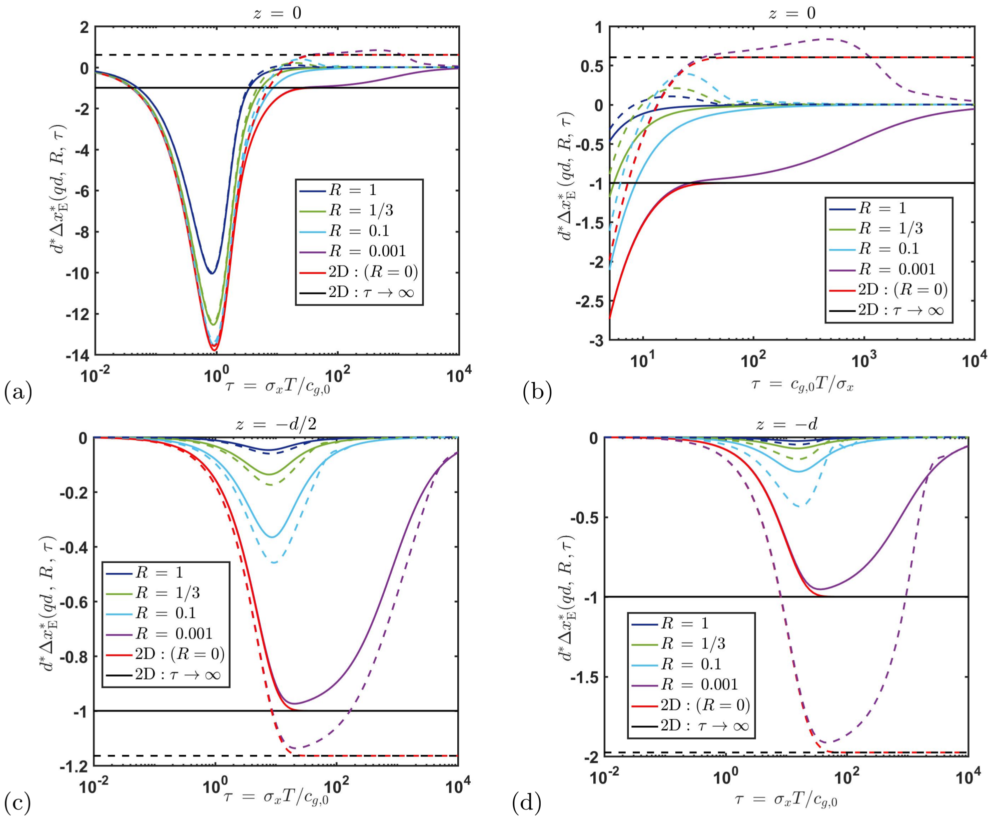

FIGURE 4. Comparison of rescaled finite-time Eulerian displacements in unstratified (solid lines) and stratified flow with stratification measure $qd = Nd/c_{g,0} = 0.6\pi$ (dashed lines) for various aspect ratios $R = \sigma_x/\sigma_y$ at $z = 0$ (panel (a), (b)), $z = -d/2$ (panel (c)) and $z = -d$ (panel (d)). Panel (b) shows a zoomed-in version of panel (a), showing τ-range from 5 to 10^4, so that the (small) difference due to stratification at the surface can be seen more clearly.

long-time limit as $R \to 0$ with displacements now enhanced by stratification to become more negative.

4. Conclusions

We have examined the Lagrangian displacement induced by surface gravity wavepackets and, in particular, the displacement associated with the wave-induced Eulerian return flow, focussing on the effects of localisation in the spanwise coordinate (as a proxy for weak directional spreading) and density stratification. For spanwise-infinite wavepackets (2D) on an unstratified flow, the net Eulerian displacement is not a function of the vertical coordinate, depending inversely on the ocean depth and becoming zero when the depth is truly infinite. In the presence of any localisation of the packet in the spanwise coordinate, the net Eulerian displacement reduces to zero. Over finite time, the return flow in 3D initially displaces particles in the same manner as in 2D, but eventually returns particles to their original positions as the flow returns around as well as underneath the packet. This transition between 2D-like and 3D-like behaviour occurs on a timescale $\sim \sigma_y/c_g$, where σ_y is the spanwise packet scale (proportional to the degree of directional spreading) and c_g is the group velocity of the surface waves.

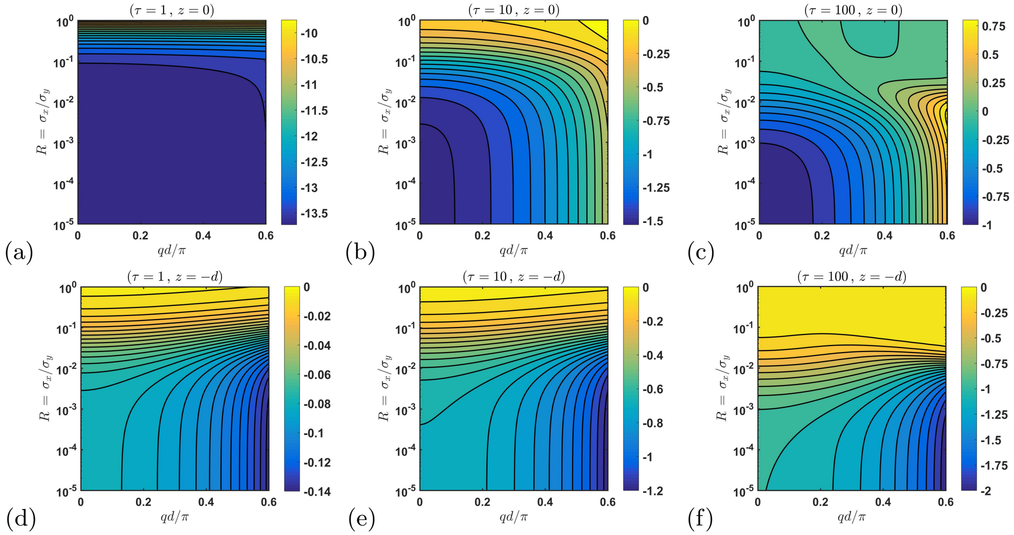

FIGURE 5. Contours of rescaled finite-time displacement $d^*\Delta x^*_{\mathrm{E}}(\tau)$ as a function of $qd/\pi = Nd/(c_{g,0}\pi)$ and $R = \sigma_x/\sigma_y$: panels (a)-(c) show the finite-time displacement at $z = 0$ and panels (d)-(f) at $z = -d$. Moving from left to right, the (packet) time $\tau = c_{g,0}t/\sigma_x$ is increased sequentially by a factor of 10, from (a) and (d) plotted at $\tau = 1$, to panels (c) and (f) plotted at $\tau = 100$.

The introduction of density stratification alters the depth profile of the net displacement by 2D packets: the net displacement becomes an oscillatory function of z, with a wavelength dependent on the parameter qd, where $q \equiv N/c_g$ is the buoyancy wavenumber, d is the ocean depth, and N is the Brunt-Väisälä frequency (assumed constant). For $qd < \pi$, as is typical for the ocean, stratification diminishes displacements near the surface and enhances them at depth. When $qd \to \pi$ (more generally, for $qd \to n\pi$), the net displacement becomes singular due to a resonance between the group velocity of the surface waves and the phase velocity of a long, x-independent internal wave mode. For $qd > \pi$, the displacement is again finite but of opposite sign. In the presence of any localisation of the packet in the spanwise coordinate, the net Eulerian displacement again reduces to zero. The finite-time displacement may be appreciably altered with the signature of the internal waves generally only present for larger times at the surface and for all times at depth.

In order to obtain a quantitative understanding of the magnitudes of the displacements, we first consider the 'displacement scale' $\alpha^2\sqrt{\pi}\sigma_x/(k_0 d)$, with $\alpha \equiv k_0 a_0$, by which we have to multiply the values (on the colour scale) in figure 5 in order to obtain dimensional displacements (in m). To consider how large this displacement scale can be, we take the largest possible value of $\alpha = 0.3$, the smallest value of $k_0 d = 3$ for the deep-water assumption to still hold, and a value of $\sigma_x = 1/(2k_0\varepsilon) = 3.1 \times 10^2\,\mathrm{m}$, corresponding to typical values $\omega_0 = 2\pi/10$, $d = 75\,\mathrm{m}$, $\varepsilon = 0.04$ (see table 1). We then obtain a displacement scale $\alpha^2\sqrt{\pi}\sigma_x/(k_0 d) = 17\,\mathrm{m}$. For a more typical value of the ocean depth of $3.1 \times 10^2\,\mathrm{m}$, this displacement scale reduces to $0.41\,\mathrm{m}$ and even further to $0.011\,\mathrm{m}$ for more typical steepness of $\alpha = 0.05$. For an unstratified flow in 2D, the displacement scale gives the dimensional value of the net displacement by the Eulerian return flow (times -1). We will now consider typical values of R and qd.

Parameter	Range	Typical value
α	$0 - 0.3$	0.05
d [m]	$3 \times 10^1 - 1.1 \times 10^4$	3.1×10^3
ω_0 $\left[\mathrm{s}^{-1}\right]$	$2\pi/20 - 2\pi/1.0$	$2\pi/10$
ε	$0 - 0.15$	0.04
σ_θ [deg]	$0 - 30$	5.0
R	$0 - 1$	4.9×10^{-3}
N $\left[\mathrm{s}^{-1}\right]$	$2\pi/\left(2.0 \times 10^3\right) - 2\pi/\left(1.3 \times 10^3\right)$	$2\pi/\left(1.3 \times 10^3\right)$
qd/π	$0 - 1$	0.6

TABLE 1. Realistic parameter ranges and typical values chosen (compiled from Haney & Young (2017); van den Bremer & Taylor (2015); Ewans (2002); Toffoli & Bitner-Gregersen (2017)).

4.1. *Quantitative effect of directional spreading*

In order to relate the value of the packet aspect ratio $R \equiv \sigma_x/\sigma_y$ to typical values of the (root-mean-square) directional spreading of the energy spectrum σ_θ reported in the literature (e.g. Ewans (2002)), we use the relationship $R \approx \sqrt{2}\varepsilon\sigma_\theta$, which is only valid in the limit of weak directional spreading. Using a value of $\sigma_\theta = 5.0°$ typical of swell conditions (Ewans 2002) and $\varepsilon = 0.04$, we obtain $R = 4.9 \times 10^{-3}$, increasing to $R = 1.9 \times 10^{-2}$ for a very narrow-banded packet with $\varepsilon = 0.15$ and further to $R = 0.11$ for a highly directionally-spread packet with $\sigma_\theta = 30°$. The timescale on which the transition from 2D-like to 3D-like behaviour occurs, $T \sim \sigma_x/(c_g R) = (R\varepsilon\omega_0)^{-1}$, can thus be as large as 8.1×10^3 s ($R = 4.9 \times 10^{-3}, \varepsilon = 0.04$) or 3.6×10^2 s ($R = 0.11, \varepsilon = 0.15$) for the typical value of $\omega_0 = 2\pi/10\,\mathrm{s}^{-1}$ considered before, with corresponding much shorter packet-translation times of $\sigma_x/c_g \approx 40$ s and 11 s, respectively.

4.2. *Quantitative effect of stratification*

Taking a typical ocean depth of 3.1×10^3 m and a (constant) value of $N = 2\pi/1333\,\mathrm{s}^{-1}$, we obtain $qd/\pi = 0.6$. The 2D net displacement by the return flow is then zero at a depth of $z = -5.0 \times 10^2$ m (cf. panel (d) of figure 3). The displacement at the surface is positive and its maximum value occurs at the ocean floor. The behaviour predicted for larger values of qd, including the resonance at $qd = n\pi$, are unlikely to arise in the real ocean. Furthermore, the depth-variability of N observed in real oceans (e.g. exponential or piecewise-linear in a crude approximation) would likely weaken the role of stratification predicted here and prevent exact resonances.

4.3. *Neglected effects: dispersion and the earth's rotation*

In this paper, we have ignored the effect of frequency dispersion by considering only leading-order terms in the small bandwidth parameter ε, and have not considered at all the earth's rotation. At the next order in ε, two effects need to be accounted for. First, we have used the rigid-lid approximation throughout this paper to neglect the set-down of the wave-averaged free surface (the quantity h_2 given by (2.5)) when calculating displacements by the return flow. In appendix A, we show that including the set-down results in a multiplication of the net displacement by at most a factor $(1 - \varepsilon^2\sigma_x/d)^{-1}$, with the largest correction occurring for a 2D shallow return flow. Even for larger values of ε this effect is small (see figure 6(b) in appendix B). Second, we have assumed that the packet propagates without any change in shape. In appendix B we find that to leading order the enhancement of displacement due to wave dispersion is $(1+\varepsilon^2/2)$, which again is small even for large values of ε (cf. figure 6(a)).

On a rotating earth, Ursell & Deacon (1950) demonstrated that an unopposed Stokes drift would violate conservation of circulation and the Lagrangian drift accompanying a regular wave train must be zero. Hasselmann (1970) showed that rotation induces a cross-wave stress on the Lagrangian current associated with periodic, deep-water surface waves, causing it to rotate and to cancel with the Stokes drift after a quarter of an inertial day; this is known as an anti-Stokes flow. As the periods associated with rotational effects are much longer than the translation timescale of the packet (see also Herbers & Janssen (2016)), we anticipate that Coriolis effects can be neglected when considering net displacements by the Eulerian return flow. Two inverse Rossby numbers for the packet play a role: $f\sigma_x/c_g$ and $f\sigma_y/c_g$. The first ($f\sigma_x/c_g$) would only be appreciably large for a very long and slow-moving packet, or for strong rotation. However, the second ($f\sigma_y/c_g$) is large for almost-unidirectional waves, leaving open the possibility that rotation may affect the mean flow over sufficiently long timescales. Since $f/N \sim 10^{-2}$ outside of the polar regions, and stratification effects scale with Nd/c_g, it is probable that in real oceans the energy transfer from the packet to the internal wave wake would dissipate the packet long before Coriolis forces act to form an anti-Stokes flow. Even in the absence of stratification, amplitude dispersion would likely have caused the packet to decay long before rotational effects become important. Strong rotation is known to affect mean flows and their associated particle dispersion in water which is shallow with respect to the surface waves (Thomas *et al.* 2018; Bühler & Holmes-Cerfon 2009). In the deep ocean, it is conceivable that rotation may influence dispersion by random second-order Lagrangian flows, which arises on longer timescales than those associated with packet translation. We hope to consider this question in future work.

Appendix A. Inclusion of the set-down

In this appendix, we consider how the set-down of the wave-averaged free surface, h_2, impacts the net displacement by a 2D return flow. We have previously used the rigid-lid approximation to neglect the set-down (given by (2.5)), which corresponds to ignoring the double time derivative on the left-hand side of (2.4) when calculating the potential for the return flow. Up to $O(\alpha^2\varepsilon^3)$ the overbarred term in (2.4) is zero and the surface forcing M remains unchanged, so only the linear operator acting on the potential ϕ_2 is altered by the inclusion of the set-down,

$$\left(\frac{c_g^2}{g}\partial_{\tilde{x}}^2 + \partial_z\right)\phi_2\bigg|_{z=0} = \partial_{\tilde{x}} M, \tag{A 1}$$

where we have moved into the group frame $\tilde{x} \equiv (x - c_g t)$. The solution to the Laplace equation which obeys the surface condition (A 1) is

$$\phi_2 = \frac{\omega_0 a_0^2 \sigma_x \sigma_y}{8\pi} \iint_{\mathbb{R}^2} \frac{ike^{-k^2\sigma_x^2/4 - l^2\sigma_y^2/4}}{\sqrt{k^2+l^2} - \frac{\varepsilon c_g^2 k^2}{g\tanh(d\sqrt{k^2+l^2})}} \frac{\cosh((z+d)\sqrt{k^2+l^2})}{\sinh(d\sqrt{k^2+l^2})} e^{ik\tilde{x}} e^{ily}\, dk dl. \tag{A 2}$$

This is almost identical to (2.15), but the denominator of the first fraction is now modified slightly due to our inclusion of the set-down term. Since $\varepsilon c_g^2 k^2/g \tanh\left(d\sqrt{k^2+l^2}\right)$ is always positive, we note that the set-down enhances the return flow. As we have shown that the net displacement disappears in 3D (cf. (2.16)) but is 2D-like for short times (cf. §2.4), we only consider the 2D displacement here. The horizontal velocity in 2D, with the set-down term included, is given by

$$u_2 = -\frac{\omega a_0^2 \sigma_x}{4\sqrt{\pi}} \int_{-\infty}^{\infty} \frac{k e^{-k^2\sigma_x^2/4}}{1 - \frac{\varepsilon c_g^2 k}{g \tanh(kd)}} \frac{\cosh\left(k\left(z+d\right)\right)}{\sinh\left(kd\right)} e^{ik\tilde{x}} dk. \tag{A 3}$$

Integrating this over all time (all $\tilde{x}/c_g$ in the group frame) results in a delta-function at $k = 0$, so the net displacement (dimensional and scaled respectively) is given by

$$\Delta x_{\mathrm{E}} = -\frac{\omega_0 a_0^2 \sqrt{\pi}}{2c_g} \frac{\sigma_x}{d} \frac{1}{\left(1 - \varepsilon c_g^2/(gd)\right)}, \qquad \Delta x_{\mathrm{E}}^* = -\frac{1}{d^*} \frac{1}{\left(1 - \varepsilon^2/(2d^*)\right)}, \tag{A 4a,b}$$

where $d^* \equiv d/\sigma_x$ is the ocean depth scale with respect to the packet scale. Inclusion of the set-down in 2D therefore results in a multiplication of the net displacement by a factor $(1 - \varepsilon c_g^2/gd)^{-1}$, which may alternatively be written as $(1 - \varepsilon^2/(2d^*))$ by using the definition $\varepsilon \equiv (2k_0\sigma_x)^{-1}$. Hence, if $k_0 d$ is large and ε is small, in such a manner that $d^* = 2\varepsilon(k_0 d) \gg 1$, it is justified to make the 'rigid-lid' approximation by neglecting $\partial_t h_2$ in (2.1b) when calculating the leading-order return flow in deep water. We note from (A 4b) that the effect of the set-down is largest when the return flow is 2D ($R = 0$) and shallow ($d^* \equiv d/\sigma_x \ll 1$); for a large bandwidth $\varepsilon = 0.125$ and a depth scale $d^* = 1/2$, the leading-order correction is about 3% (see figure 6b). While this correction increases as d^* decreases we note that, since $d^* = 2\varepsilon(k_0 d)$, we must have $d^*/\varepsilon \gg 1$ to avoid violating the deep-water assumption.

The Stokes drift is not sensitive to the second-order set-down, as it is calculated using the linear waves and free surface profile. Including the set-down in the calculation of net Eulerian displacement, we find that the depth-integral of (dimensional) Lagrangian net displacement is no longer zero as in (2.13) but negative,

$$\int_{-d}^{0} \Delta x_{\mathrm{L}} dz = -\alpha^2 \varepsilon^2 \frac{\sigma_x^2 \sqrt{\pi}}{k_0 d} + O\left(\varepsilon^4\right). \tag{A 5}$$

This slight mass imbalance occurs because the Eulerian return flow forced by the divergence of the Stokes transport is just a part of the overall mass-conserving system, which must take into account the changes in mean level far from the packet at this order in ε. Note that as $k_0 d \to \infty$ (and hence $d/\sigma_x \to \infty$ for a finite ε) this mass imbalance disappears, in agreement with McIntyre (1981).

Appendix B. The leading-order effect of dispersion

In this appendix, we explore the leading-order effect of wave dispersion on the net Lagrangian displacement in unstratified flow, over times t satisfying $\varepsilon^2 t = O(1)$. To do so, we update the linear quantities (2.2) to include dependence on a slow timescale $T = \varepsilon^2 t$ in §B.1 (see also e.g. (Kinsman 2002)), and in §B.2 we determine the mean-flow forcing equation (2.4) at $O(\alpha^2\varepsilon^2)$ accordingly. We then assume a shallow return flow, and examine the 2D case and 3D case in §B.3 and §B.4 respectively.

B.1. *First-order solutions $O(\alpha)$*

From the combined linear boundary condition $(\partial_t^2 + g\partial_z)\phi_1 = 0$ at $z = 0$, we first obtain an evolution equation for A_0 in terms of the slow timescale at $O(\varepsilon^2)$, as well as its Fourier-space solution,

$$\partial_T A_0 = i\frac{c_g^2}{2\omega_0} \partial_{\tilde{x}\tilde{x}} A_0, \qquad \hat{A}_0(k,l,T) = \hat{A}_0(k,l) e^{ik^2\gamma_0 T/2}, \tag{B 1a,b}$$

where $\gamma_0 \equiv \partial^2\omega_0/\partial k^2|_{k=k_0} = -\sqrt{g/k_0^3}/4$ is the dispersive parameter. Inverting the Fourier transform in (B 1b), the surface profile in real space is found to maintain a Gaussian shape which evolves on the slow, dispersive timescale,

$$A_0\left(x,y,T\right) = a_0^{\text{Disp}} e^{-\tilde{x}^2/\left(2\left(\sigma_x^{\text{Disp}}\right)^2\right)} e^{-y^2/\left(2\sigma_y^2\right)}, \tag{B 2}$$

where the 'Disp' superscript denotes the inclusion of leading-order dispersion, and the slowly-varying parameters are

$$a_0^{\text{Disp}} = \frac{a_0}{\sqrt[4]{1+\gamma_0^2 t^2/\sigma_x^4}}, \qquad \sigma_x^{\text{Disp}} = \sigma_x\sqrt{1+\gamma_0^2t^2/\sigma_x^4}. \tag{B 3a,b}$$

Dispersion is hence important for times $t \geqslant \sigma_x^2/|\gamma_0|$. Over time, the packet decreases in amplitude and widens as it translates at the group velocity c_g of the waves. It is therefore not steady in its own reference frame.

B.2. *Second-order solutions $O(\alpha^2)$*

Considering the discussions in appendix A, and the conclusion that the set-down contribution is $O(\varepsilon^2/d^*)$, we will include the ∂_t^2 term on the left-hand side of (2.4), whilst emphasising that this term is due to the set-down rather than dispersion. It is found that the terms of $O(\alpha\varepsilon)$ in (2.2a,b) do not contribute to the right-hand side of (2.4) at $O(\alpha^2\varepsilon^2)$; the wave forcing terms obtained by multiplying the $O(\alpha\varepsilon)$ by the $O(\alpha\varepsilon^0)$ terms in (2.2) disappear under wave-averaging. Consequently, we only need to update the functional dependence of A_0 to include evolution on the slow, dispersive timescale $T = \varepsilon^2 t = O(1)$ in order to calculate the updated M. At $O(\alpha^2\varepsilon^2)$, the mean flow is therefore still forced solely by the Stokes transport, which is now slowly evolving. The boundary condition for the Laplace equation satisfied by ϕ_2 is similar to (A 1) but with an updated, dispersive M,

$$\left(\frac{c_g^2}{g}\partial_{\tilde{x}}^2 + \partial_z\right)\phi_2^{\text{Disp}}\bigg|_{z=0} = \partial_{\tilde{x}} M^{\text{Disp}}. \tag{B 4}$$

Solving (B 4) in Fourier space, we obtain

$$\phi_2^{\text{Disp}} = \frac{\omega_0|a_0^{\text{Disp}}|^2\sigma_x^{\text{Disp}}\sigma_y}{8\pi}\iint_{\mathbb{R}^2} \frac{ike^{-k^2\left(\sigma_x^{\text{Disp}}\right)^2/4-l^2\sigma_y^2/4}}{\sqrt{k^2+l^2}-\frac{\varepsilon c_g^2k^2}{g\tanh(d\sqrt{k^2+l^2})}}\frac{\cosh((z+d)\sqrt{k^2+l^2})}{\sinh(d\sqrt{k^2+l^2})}e^{ik\tilde{x}}e^{ily}dkdl. \tag{B 5}$$

For simplicity in subsequent calculations, we assume a shallow return flow, and hence we must include the set-down term.We consider a particle beneath the centre of the packet $(x,y) = (0,0)$ at $t = 0$, and obtain from (B 5)

$$u_2^{\text{Disp}} = -\frac{\omega_0 a_0^2}{8\pi d}\iint_{\mathbb{R}^2}\frac{\kappa^2 e^{-\kappa^2/4}e^{-\lambda^2/4}}{\kappa^2\left(1-\varepsilon^2/d^*\right)+R^2\lambda^2}e^{-\varepsilon^2\kappa^2\hat{t}^2/4}e^{-i\kappa\hat{t}}d\kappa d\lambda, \tag{B 6}$$

where $\kappa \equiv k\sigma_x$, $\lambda \equiv l\sigma_y$, $\hat{t} = c_{g,0}t/\sigma_x$ and $d^* \equiv d/\sigma_x$. We will now consider the displacement in 2D and 3D in turn.

B.3. *The dispersive time integral in 2D*

In the special case of a 2D shallow return flow ($R = 0$), the velocity (B 6) may be written in real space,

$$u_2^{\text{Disp}} = -\frac{\omega_0 a_0^2}{2d\left(1-\varepsilon^2/d^*\right)}\frac{e^{-\frac{\hat{t}^2}{1+\varepsilon^2\hat{t}^2}}}{\sqrt{1+\varepsilon^2\hat{t}^2}}. \tag{B 7}$$

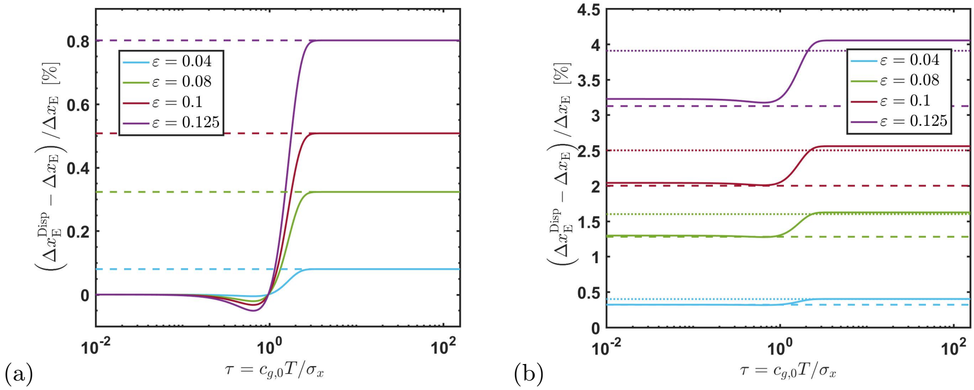

FIGURE 6. Percentage change of the 2D finite-time Eulerian displacement for a shallow return flow due to dispersion alone (panel (a)) and dispersion with a set-down (panel (b)), for different bandwidth parameters ε and at a fixed depth scale $d^* \equiv d/\sigma_x = 1/2$ obtained from numerical integration of (B 7) (continuous lines). In panel (a), the leading-order corrections to net displacement due to dispersion alone ($\varepsilon^2/2$) are shown as a dashed lines. In panel (b), the leading-order corrections to net displacement due to the set-down (ε^2/d^*) and the total leading-order corrections ($\varepsilon^2/d^* + \varepsilon^2/2$) are shown as dashed and dotted lines, respectively.

The integral to compute the 2D finite-time Eulerian displacement is given by

$$\Delta x_{\mathrm{E}}^{\mathrm{Disp}}(\tau) = \frac{-2D(\tau,\varepsilon)}{\sqrt{\pi}d^*\left(1-\varepsilon^2/d^*\right)} \quad \text{with} \quad D(\tau,\varepsilon) = \int_0^{\tau} \frac{e^{-\frac{\hat{t}^2}{1+\varepsilon^2\hat{t}^2}}}{\sqrt{1+\varepsilon^2\hat{t}^2}} d\hat{t}, \qquad \text{(B 8a,b)}$$

where we have evaluated a single half of the symmetric time integral. The integral $D(\tau,\varepsilon)$ does not converge in the long-time limit $\tau \to \infty$, giving an infinite net displacement. To show this, we transform the integral (B 8b) into a form that separates the divergent and convergent contributions using the change of variables $s^2/\varepsilon^2 = t^2/\left(1+\varepsilon^2 t^2\right)$. As we are interested in the limit $\tau \to \infty$ (corresponding to $s \to 1$), we set the upper limit to be $s = 1-\delta$, where δ is a small parameter, and obtain from (B 8b)

$$D(\tau,\varepsilon) = \frac{e^{-\frac{1}{\varepsilon^2}}}{\varepsilon}\int_0^{1-\delta}\frac{ds}{1-s^2} + \frac{1}{\varepsilon}\int_0^{1-\delta}\left(e^{-\frac{s^2}{\varepsilon^2}} - e^{-\frac{1}{\varepsilon^2}}\right)\left(1+s^2+O(s^4)\right)ds, \qquad \text{(B 9)}$$

where we have used a standard Taylor-series expansion for $s^2 < 1$ in the second integral of (B 9). Performing both integrations (the latter by parts) results in the following approximation to (B 8b),

$$D(\tau,\varepsilon) = \frac{e^{-\frac{1}{\varepsilon^2}}}{2\varepsilon}\log\left(\frac{2}{\delta}\right) + \frac{\sqrt{\pi}}{2}\left(1+\frac{\varepsilon^2}{2}\right)\operatorname{erf}\left(\frac{1}{\varepsilon}\right) - \frac{e^{-\frac{1}{\varepsilon^2}}}{\varepsilon}\left(2+\frac{1}{3}+\ldots\right) + O\left(\varepsilon^4, \frac{\delta}{2}\right). \qquad \text{(B 10)}$$

To ensure consistency, we can readily recover the non-dispersive net displacement from (B 10) as $\varepsilon \to 0$ ($D \to \sqrt{\pi}/2$ and $\Delta x_{\mathrm{E}}^{\mathrm{Disp}} \to -1/d^*$ from (B 8a)). All terms to the right of $\operatorname{erf}(1/\varepsilon)$ must be neglected since they are either higher-order (or beyond all orders) in ε or proportional to δ. In the long-time limit of $\delta \to 0^+$, the logarithm in (B 10) is the divergent term. We can estimate how small δ must be for this to become significant, namely $\delta \sim \exp\left(-\varepsilon\exp\left(\varepsilon^{-2}\right)\right)$, which is minuscule for small ε. From the variable transformation $s^2/\varepsilon^2 = t^2/\left(1+\varepsilon^2 t^2\right)$, we obtain that for large times $\delta \approx 1/(2\varepsilon^2\tau^2)$. Using this estimate, we find that the integral begins to diverge at $\tau^* \sim \varepsilon^{-1}\exp\left(\varepsilon\exp\left(\varepsilon^{-2}\right)\right)$, which is extremely large for $\varepsilon \ll 1$.

In order for δ to be small when $\varepsilon\tau$ is large, we must have that $\tau \geqslant \varepsilon^{-2}$, corresponding to times over which previously ignored higher-order dispersive effects become significant. It follows that δ is at most $\varepsilon^2/2$ for large times. Neglecting the logarithmic term but keeping the leading-order terms in (B 10) may then be thought of as a formal truncation of the integral at some intermediate time $\varepsilon^{-2} < \tau \ll \tau^*$, and we obtain

$$\Delta x_{\mathrm{E}}^{\mathrm{Disp}} = -\frac{1}{d^*\left(1-\varepsilon^2/d^*\right)}\left(1+\frac{\varepsilon^2}{2}\right) + O\left(\varepsilon^4\right) = -\frac{1}{d^*}\left(1+\frac{\varepsilon^2}{d^*}+\frac{\varepsilon^2}{2}\right) + O\left(\varepsilon^4\right). \quad \text{(B 11)}$$

It is clear from (B 11) that dispersion enhances the 2D Eulerian displacement, as is shown in figure 6(a) for different values of the bandwidth parameter ε. The correction due to the set-down (ε^2/d^*, to leading order) is present for all time, whereas the dispersive correction ($\varepsilon^2/2$ in (B 11)) arises on a time scale $\tau = O(10^1) - O(10^2)$ (see figure 6(b)). For large ε, terms of order $\left(\varepsilon^2/d^*\right)^2$ are responsible for the solid lines ending above the dotted lines in figure 6(b).

Calculating the net Stokes displacement involves the same time-integral as in (B 8), resulting in the dispersive modification

$$\Delta x_{\mathrm{S}}^{*\mathrm{Disp}} = \left(1+\frac{\varepsilon^2}{2}\right) 2k_0\sigma_x e^{2k_0 z} + O\left(\varepsilon^4\right). \quad \text{(B 12)}$$

If the set-down is not present, the depth-integral of the net Lagrangian displacement remains zero even with leading-order dispersion accounted for. The dispersive correction $1+\varepsilon^2/2+O(\varepsilon^4)$ does not depend on the depth structure of the return flow, which may be seen from the evaluation of the time integral in the following section.

B.4. *The dispersive time integral in 3D*

The 3D shallow return flow integral cannot be fully evaluated analytically, so the displacement is expressed as the triple integral (with $\hat{t}$ dimensionless packet-time),

$$\Delta x_{\mathrm{E}}^{\mathrm{Disp}} = -\frac{2}{\pi^{3/2} d^*}\int_0^\infty\int_0^\infty\int_0^\tau \frac{\kappa^2 e^{-\frac{\kappa^2}{4}} e^{-\frac{\lambda^2}{4}}}{\kappa^2\left(1-\varepsilon^2/d^*\right)+R^2\lambda^2} e^{-\frac{\varepsilon^2\kappa^2\hat{t}^2}{4}} \cos\left(\kappa\hat{t}\right) d\kappa d\lambda d\hat{t}. \quad \text{(B 13)}$$

Using complex exponentials, we can first exactly evaluate the finite-time integral

$$\int_0^\tau e^{-\frac{\varepsilon^2\kappa^2\hat{t}^2}{4}} \cos\left(\kappa\hat{t}\right) d\hat{t} = \frac{\sqrt{\pi}}{2\kappa}\frac{e^{-\frac{1}{\varepsilon^2}}}{\varepsilon} \mathrm{Re}\left\{\mathrm{erf}\left(\frac{\varepsilon\kappa\tau}{2}+\frac{i}{\varepsilon}\right)\right\}. \quad \text{(B 14)}$$

In the long-time limit, (B 14) is dominated by its behaviour near $\kappa = 0$, and so $\varepsilon\kappa\tau \ll 1/\varepsilon$ when τ is sufficiently large. By expanding the error function for $\varepsilon\kappa\tau \ll 1/\varepsilon$ and taking $\exp(-\varepsilon^2\kappa^2\tau^2/4) \approx 1$, the same dispersive correction of 2D is obtained (cf. (B 10)),

$$\frac{\sqrt{\pi}e^{-\frac{1}{\varepsilon^2}}}{2\varepsilon}\mathrm{Re}\left\{\frac{1}{\kappa}\,\mathrm{erf}\left(\frac{\varepsilon\kappa\tau}{2}+\frac{i}{\varepsilon}\right)\right\} = \frac{\sin(\kappa\tau)}{\kappa}\left(1+\frac{\varepsilon^2}{2}+O(\varepsilon^4)\right). \quad \text{(B 15)}$$

The condition $\varepsilon\kappa\tau \ll 1/\varepsilon$ suggests that for $\kappa = O(1)$ we should truncate the long-time integral when $\varepsilon^{-2} < \tau \ll \tau^*$ to be consistent with the separation of scales expansion (as in the 2D case). In general, this regime for τ corresponds to a certain κ-interval. While the net displacement remains zero in 3D ($\sin(\kappa\tau)/\kappa$ tends to $\pi\delta(\kappa)$ as $\tau \to \infty$), dispersion weakly enhances the finite-time Eulerian displacement, which is obtained as

$$\Delta x_{\mathrm{E}}^{\mathrm{Disp}}(\tau) = -\frac{2}{d^*\pi^{3/2}}\left(1+\frac{\varepsilon^2}{2}\right)\int_0^\infty\int_0^\infty \frac{\kappa\sin\left(\kappa\tau\right) e^{-\frac{\kappa^2}{4}} e^{-\frac{\lambda^2}{4}}}{\kappa^2\left(1-\varepsilon^2/d^*\right)+R^2\lambda^2} d\kappa d\lambda + O(\varepsilon^4). \quad \text{(B 16)}$$

We note that no assumption on the depth structure of the flow was required to obtain the dispersive corrections. As with the non-dispersive integral in (2.23), the λ integral in (B 16) can now be performed, leading to an expression similar in form to (2.24) but slightly modified by the set-down term and multiplied by the dispersive correction.

REFERENCES

Bühler, O. 2014. *Waves and Mean Flows*. 2nd edn. Cambridge University Press, Cambridge, UK.

Bühler, O., & Holmes-Cerfon, M. 2009. Particle dispersion by random waves in rotating shallow water. *J. Fluid Mech.*, **638**, 5–26.

Christensen, K. H., & Terrile, E. 2009. Drift and deformation of oil slicks due to surface waves. *J. Fluid Mech.*, **620**, 313–332.

Davey, A., & Stewartson, K. 1974. On three-dimensional packets of surface waves. *Proc. Roy. Soc. A*, **338**(1613), 101–110.

Drivdal, M., Broström, G., & Christensen, K. H. 2014. Wave-induced mixing and transport of buoyant particles: application to the Statfjord A oil spill. *Ocean Science*, **10**(6), 977–991.

Dysthe, K. B. 1979. Note on a modification to the nonlinear Schrödinger equation for application to deep water waves. *Proc. Roy. Soc. London A*, **369**(1736), 105–114.

Ewans, K. 2002. Directional spreading in ocean swell. *Pages 517–529 of: Fourth International Symposium on Ocean Wave Analysis and Measurement*.

Haney, S., & Young, W. R. 2017. Radiation of internal waves from groups of surface gravity waves. *J. Fluid Mech.*, **829**, 280–303.

Hasselmann, K. 1962. On the non-linear energy transfer in a gravity-wave spectrum. Part 1. General theory. *J. Fluid Mech.*, **12**(4), 481–500.

Hasselmann, K. 1970. Wave-driven inertial oscillations. *Geophys. Fluid Dyn.*, **1**, 463–502.

Herbers, T. H. C., & Janssen, T. T. 2016. Lagrangian surface wave motion and Stokes drift fluctuations. *J. Phys. Oceanogr.*, **46**(4), 1009–1021.

Herterich, K., & Hasselmann, K. 1982. The horizontal diffusion of tracers by surface waves. *J. Phys. Oceanogr.*, **12**(7), 704–711.

Jones, C. E., Dagestad, K., Breivik, Ø., Holt, B., Röhrs, J., Christensen, K., Espeseth, M., Brekke, C., & Skrunes, S. 2016. Measurement and modelling of oil slick transport. *J. Geophys. Res.*, **121**(10), 7759–7775.

Kinsman, B. 2002. *Wind Waves: Their Generation and Propagation on the Ocean Surface*. Dover. N.Y.

Lebreton, L., Slat, B., Ferrari, F., Sainte-Rose, B., Aitken, J., Marthouse, R., Hajbane, S., Cunsolo, S., Schwarz, A., Levivier, A., Noble, K., Debeljak, P., Maral, H., Schoeneich-Argent, R., Brambini, R., & Reisser, J. 2018. Evidence that the Great Pacific Garbage Patch is rapidly accumulating plastic. *Scientific Reports*, **8**, 4666.

Longuet-Higgins, M. S., & Stewart, R. W. 1962. Radiation stress and mass transport in gravity waves, with application to 'surf beats'. *J. Fluid Mech.*, **13**(4), 481–504.

Longuet-Higgins, M.S. 1953. Mass transport in water waves. *Phil. Trans. Roy. Soc. London A*, **245**(903), 535–581.

Longuet-Higgins, M.S. 1957. The statistical analysis of a random, moving surface. *Phil. Trans. Roy. Soc. London A*, **249**(966), 321–387.

McAllister, M. L., Adcock, T. A. A., Taylor, P. H., & van den Bremer, T. S. 2018. The set-down and set-up of directionally spread and crossing surface gravity wave groups. *J. Fluid Mech.*, **835**, 131–169.

McIntyre, M. E. 1981. On the 'wave momentum' myth. *J. Fluid Mech.*, **106**, 331–347.

McIntyre, M.E. 1980. An introduction to the generalized Lagrangian-mean description of wave, mean-flow interaction. *Pure Appl. Geophys.*, **118**(1), 152–176.

Phillips, O.M. 1977. *The dynamics of the upper ocean*. Cambridge University Press.

Röhrs, J., Christensen, K. H., Hole, L. R., Broström, G., Drivdal, M., & Sundby, S. 2012. Observation-based evaluation of surface wave effects on currents and trajectory forecasts. *Ocean Dynamics*, **62**(10), 1519–1533.

Stokes, G. G. 1847. On the Theory of Oscillatory Waves. *Trans. Cam. Phil. Soc.*, **8**, 441–455.

Thomas, J., Bühler, O., & Shafer Smith, K. 2018. Wave-induced mean flows in rotating shallow water with uniform potential vorticity. *J. Fluid Mech.*, **839**, 408–429.

Toffoli, A., & Bitner-Gregersen, E.M. 2017. *Types of ocean surface waves, wave classification.* John Wiley & Sons, Ltd. Pages 1–8.

Trinanes, Joaquin A., Olascoaga, M. Josefina, Goni, Gustavo J., Maximenko, Nikolai A., Griffin, David A., & Hafner, Jan. 2016. Analysis of flight MH370 potential debris trajectories using ocean observations and numerical model results. *Journal of Operational Oceanography*, **9**(2), 126–138.

Ursell, F., & Deacon, G. 1950. On the theoretical form of ocean swell on a rotating earth. *Mon. Not. Roy. Astron. Soc., Geophys. Suppl.*, **6**(s1), 1–8.

van den Bremer, T. S., & Taylor, P. H. 2015. Estimates of Lagrangian transport by surface gravity wave groups: The effects of finite depth and directionality. *J. Geophys. Res.*, **120**(4), 2701–2722.

van den Bremer, T. S., & Taylor, P. H. 2016. Lagrangian transport for two-dimensional deep-water surface gravity wave groups. *Proc. Roy. Soc. London A*, **472**(2192).